CMB component separation in the pixel domain

A. Doroshkevich and O. Verkhodanov

Phys. Rev. D **83**, 043002 — Published 7 February 2011

DOI: 10.1103/PhysRevD.83.043002

DV10787

CMB component separation in the pixel domain

A. Doroshkevich[1] and O. Verkhodanov[2]

[1]*Astro Space Center of Lebedev Physical Institute of Russian Academy of Sciences, 117997 Moscow, Russia*
[2]*Special astrophysical observatory, Nizhnij Arkhyz, Karachaj-Cherkesia, Russia*

We show that the popular ILC approach is unstable with respect to division of the observed map pixels to a set of 'homogeneous' subsamples. For various choices of such subsamples we can obtain a restored CMB signal with amplitudes ranging from zero to the amplitude of the observed signal. We propose an approach which allows us to obtain corrected estimates of the CMB power spectrum, C_ℓ, at $\ell \leq 30$ and provides results similar to WMAP for larger ℓ. Using this approach, we eliminate some anomalies of the WMAP results. In particular, our estimate of the quadrupole is consistent with the theoretically expected one. The effect of the 'axis of evil' is suppressed and the symmetry of the north and south galactic hemispheres increases. These results can change estimates of quadrupole polarization and the redshift of reionization of the Universe. We also propose a new simple approach which can improve the WMAP estimates of the high ℓ power spectrum.

I. INTRODUCTION

During last years, fundamental results have been obtained from the analysis of fluctuations of relic radiation [1–9] observed by the WMAP mission. The key problem of such analysis is the separation of the cosmic microwave background (CMB) component from the Galactic foreground in the pixel domain. Several approaches have been used to determine the CMB signal from the observed map. They are the internal linear combination (ILC) and the maximum entropy methods [4, 10], the blind and Wiener filtering methods [11, 12], the Correlated Component Analysis [13], the harmonic ILC [14], the fast independent component analysis (FASTICA) [15] etc. Among these approaches the ILC method is very convenient because it requires minimal additional assumptions regarding the foreground and the separated signals. It is used in the WMAP analysis of low ℓ multipoles and is considered in details in [4, 10]. The instability of such a reconstruction owing to the correlation between the CMB and foreground was shown in [16]. Recently some problems associated with this method were discussed in [17].

In the Planck review [18], the final component separation pipeline for the Planck mission is considered. This involves a combination of methods and iterations associated with processing steps targeted at different objectives such as the diffuse component separation, spectral estimation, and compact source extraction

At the same time, some anomalies in the results of the WMAP team are widely discussed. Among these are the small amplitude of the quadrupole component, the unexpected correlation between the components with $\ell = 2\,\&\,3$ ('axis of evil'), the noticeable asymmetry between the north and south galactic hemispheres and the existence of few deep walls in the CMB map etc. Concluding discussions are given in [19] where all these anomalies are explained as random fluctuations.

A special problem is the analysis of an inhomogeneous map for which the amplitude of the foreground varies strongly over the map. In this case the analysis becomes more complex and as described in [4], it includes the division of the map into a set of more homogeneous regions, for which the component separation is performed independently. In [4] the analysis for 12 regions is presented. However, various definitions of 'homogeneous' subsamples are possible that lead to different final CMB maps and power spectra of the temperature fluctuations C_ℓ.

In this paper we show that the ILC method is unstable with respect to the definition of 'homogeneous' regions. As is shown below different criteria for homogeneity and corresponding division of the full sample of map pixels into a set of 'homogeneous' subsamples lead to different CMB maps and C_ℓ. Thus, for a different procedure we can obtain a CMB signal with arbitrary amplitude ranging from zero to the amplitude of the observed signal.

In Section 2 we represent four different procedures which can be used to divide the map pixels into a set of 'homogeneous' subsamples with analytical and numerical estimates of the efficiency of the component separation. In Section 3 we apply our "best" approach to the observed Q and V channels of WMAP and show that we can suppress some of the anomalies noted above. Section 4 includes the summary of our results and a discussion of methodological problems. In particular, we propose a new approach for the analysis of high ℓ power spectrum, which can improve now available results.

II. SEPARATION OF THE CMB SIGNAL WITH THE ILC APPROACH

Each pixel of the observed map contains a combination $S(\theta_i)$ of the CMB signal $C(\theta_i)$ and the foreground $F(\theta_i)$. Let us consider two observed maps obtained for two different frequencies. For these maps the measured signals in the i^{th} pixel, $S_1(\theta_i)\,\&\,S_2(\theta_i)$, are

$$S_1(\theta_i) = C(\theta_i) + F_1(\theta_i)\,, \qquad (1)$$

$$S_2(\theta_i) = C(\theta_i) + F_2(\theta_i).$$

Here the CMB signal $C(\theta_i)$ is the same for both channels but contributions of the foreground, $F_1\,\&\,F_2$, are differ-

ent. The ILC extraction of the CMB signal assumes that

$$C(\theta_i) = \alpha S_1(\theta_i) + (1-\alpha) S_2(\theta_i)$$

$$= S_2(\theta_i) + \alpha [S_1(\theta_i) - S_2(\theta_i)]\,, \qquad (2)$$

The minimal dispersion of the separated CMB signal (2), σ_C, is achieved for

$$\alpha = -\langle Q_2 Q_{12}\rangle / \langle Q_{12}^2\rangle\,, \qquad (3)$$

$$\sigma_C^2 = \langle C^2\rangle - \langle C\rangle^2 = \langle Q_2^2\rangle - \langle Q_2 Q_{12}\rangle^2 / \langle Q_{12}^2\rangle\,,$$

where $\langle\rangle$ means the averaging over the considered subsample of pixels. We use notation

$$Q_1(\theta_i) = S_1(\theta_i) - \langle S_1\rangle, \quad Q_2(\theta_i) = S_2(\theta_i) - \langle S_2\rangle\,,$$

$$Q_{12}(\theta_i) = Q_1(\theta_i) - Q_2(\theta_i)\,.$$

and $\langle Q_1\rangle = \langle Q_2\rangle = 0$.

However, as is seen from (1 & 2), for one pixel

$$\alpha = \alpha_f = (1 - F_1/F_2)^{-1}\,, \qquad (4)$$

and for a subsample of pixels

$$\alpha \approx \langle \alpha_f\rangle = (1 - \langle F_1/F_2\rangle)^{-1}\,, \qquad (5)$$

where α is consider as a constant in accordance with the main ideas of the ILC approach.

The relations (4 & 5) give the exact solution for the case $F_1/F_2 = const.$ and the best solution for the subsample of pixels with $F_1/F_2 \approx const.$ In that case the errors in C_i are determined by the scatter of F_1/F_2 for the subsample used. This means that in order to improve the separation we must divide the full sample of pixels into a set of more homogeneous subsamples using the distribution of the ratio $F_1(\theta_i)/F_2(\theta_i)$. After the component separation within these subsamples, we get the set of cleaned pixels which form together the cleaned map. Model 1 gives below an example of such component separation.

However, such approach cannot be used in practice as the foregrounds are *a priori* unknown and for the component separation we would have to use criteria expressed through the observed signals, S_1 & S_2. As we show below the cleaned map strongly depends upon these criteria.

For simplicity, in the further analysis we consider the pixels as independent ones and ignore the possible correlations of the measured signal and/or the separated CMB in the neighboring pixels. The inclusion of such correlations allows to improve the component separation but makes the procedure of separation more complex.

We consider below both analytically and numerically four models of map division into 'homogeneous' subsamples prepared with various definitions of 'homogeneity' (9, 12, 15, 18). To do this, we introduce a function G of the amplitudes of two signals

$$G_i = G(\theta_i) = G(S_1(\theta_i), S_2(\theta_i))$$

and distribute all pixels over a set of bins with the same size Δ, so that

$$i\,\Delta \le G_i(\theta_j) \le (i+1)\Delta\,.$$

The i^{th} bin contains J_i pixels with

$$\langle G_i\rangle = \frac{1}{J_i}\sum_{j=1}^{J_i} G_i(\theta_j)\,, \qquad (6)$$

$$|\delta_j| = |G_i(\theta_j) - \langle G_i\rangle| \le \Delta, \quad \langle \delta_i\rangle = \langle G_i - \langle G_i\rangle\rangle \equiv 0\,.$$

We consider these J_i pixels as the 'homogeneous' subsample, for which we get α_i and the CMB signal, $C(\theta_j)$, using the standard relations (3) and (2). This approach is similar to that used in [4] where the 12 pixel subsamples were selected. In contrast, we consider up to few thousand subsamples for smaller Δ.

Our analysis confirms that the exact separation of the CMB signal can be obtained only for *a priori* known foregrounds. In all other cases, we can obtain approximate estimates of this signal only. But deviations between the input and restored CMB signals depend upon the criteria for homogeneity and the accepted value Δ. For larger Δ all models give comparable results.

The next step in the analysis is the standard decomposition of the CMB map in spherical harmonics which allows us to obtain the amplitudes, a_{lm}, and the power spectrum of the CMB fluctuations

$$C_\ell = \frac{1}{2\ell+1}\sum_{m=-\ell}^{\ell} a_{\ell m}^2, \quad \Delta T_\ell^2 = \frac{\ell(\ell+1)}{2\pi} C_\ell \qquad (7)$$

A. Four models for the separation of the CMB signal

Theoretical consideration reveals the main influences of the selection criteria but real estimates of the quality of separation can be found with simulations only. To test the various methods of component separation, we generate the CMB signals with the standard power spectrum and Gaussian distribution of random amplitudes; using the foregrounds from the WMAP publications [20] we transform the generated CMB signals to observed ones and separate out the CMB signals with various approaches. The comparison of the introduced and restored power spectra C_ℓ characterizes the precision achieved with such separations for the full map.

1. Model 1

As is seen from (2 & 5) for samples with

$$F_1(\theta_i)/F_2(\theta_i) = const\,, \qquad (8)$$

we get exactly restored $C(\theta_i)$. Similar estimates result for a subsample with

$$G(\theta_i) = F_1(\theta_i)/F_2(\theta_i) = 1 + \beta + \delta(\theta_i)\,, \qquad (9)$$

$$\langle G\rangle = 1+\beta, \quad |\delta| \le \Delta, \quad \langle\delta\rangle = 0\,,$$

$$F_1 = F_2(1+\beta+\delta_i), \quad \langle Q_{12}\rangle = \beta\langle F_2\rangle + \langle F_2\delta\rangle\,.$$

Here $1+\beta$ is the center of the subsample and $\delta_i = \delta(\theta_i)$ characterizes a (small) random scatter of the pixel amplitudes with respect to the central point.

For such subsample, we get

$$\alpha = -\frac{1+o(\delta)}{\beta+o(\delta)}, \quad \alpha_f = -\frac{1}{\beta}\,,$$

and for $\delta \to 0$ we have $\alpha \to \alpha_f = -1/\beta$. In this case the scatter of the restored CMB signal is

$$\Delta_C(\theta_i) = F_2(\theta_i)\frac{\langle F_2\delta\rangle/\langle F_2\rangle + \delta(\theta_i)}{\beta+\delta(\theta_i)} \propto \delta\,.$$

$$\Delta_C(\theta_i) \to 0 \quad \text{for} \quad \delta \to 0 \qquad (10)$$

For such a choice of pixel subsamples, we get the most accurate component separation. Its precision depends upon the bin size, Δ, and increases for smaller Δ. Numerical simulations confirm this conclusion.

2. Model 2

For the sample with

$$S_1(\theta_i)/S_2(\theta_i) = const\,, \qquad (11)$$

we get the exact solution $C(\theta_i) = 0$ as in this case conditions (8) and (11) become equivalent. Similar inferences are valid also for a subsample with

$$G_i = S_1(\theta_i)/S_2(\theta_i) = 1+\beta+\delta(\theta_i), \quad |\delta| \le \Delta \quad (12)$$

Here again $1+\beta$ is the center of the subsample and $\delta(\theta_i)$ characterizes a (small) random scatter of the pixel amplitudes with respect to the central point. In this case

$$S_1(\theta_i) - S_2(\theta_i) = S_2(\theta_i)(\beta+\delta_i), \quad Q_2(\theta_i) = S_2(\theta_i) - \langle S_2\rangle\,,$$

$$Q_{12}(\theta_i) = \beta Q_2(\theta_i) + S_2(\theta_i)\delta(\theta_i) - \langle S_2\delta\rangle \qquad (13)$$

$$\langle Q_{12}^2\rangle = \beta^2\langle Q_2^2\rangle + 2\beta\langle\delta S_2 Q_2\rangle + o(\delta^2), \quad \langle\delta\rangle = 0\,,$$

$$\langle Q_2 Q_{12}\rangle = \beta\langle Q_2^2\rangle + \langle\delta S_2 Q_2\rangle, \quad \alpha \approx -1/\beta + o(\delta)\,.$$

Therefore,

$$C(\theta_i) = S_2(\theta_i)\frac{\langle\delta S_2 Q_2\rangle + o(\delta^2)}{\beta\langle Q_2^2\rangle + o(\delta)} \propto o(\delta)\,, \qquad (14)$$

$$\sigma_C^2 = \langle Q_2^2\rangle\left[1 - \frac{1+o_1(\delta)}{1+o_2(\delta)}\right] \propto o(\delta)\,.$$

Thus, we see that for $\Delta \to 0$ we have $C(\theta_i) \to 0$, $\sigma_C^2 \to 0$. For such pixel subsamples we get the extremal result – the CMB signal tends to zero. The same result can be obtained for an arbitrary function $G = G(S_1/S_2)$. Numerical models confirm this tendency.

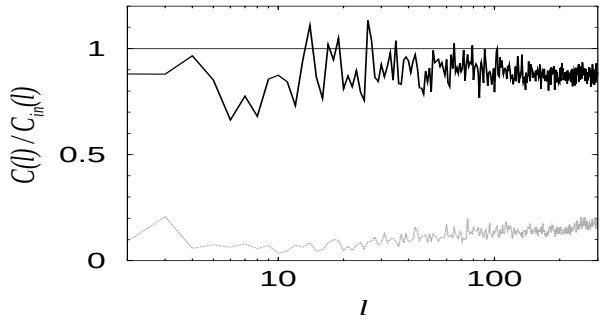

FIG. 1. For the model 2, two reconstructions of the simulated CMB signal are plotted for the foregrounds in Q and V bands. Results are normalized on the input signal and are shown for $\Delta = 2\,\&\,0.2$ (solid and dashed lines).

3. Model 3

As a next interesting example, we consider the subsample of pixels with

$$G_i = S_1(\theta_i) = S_0[1+\delta(\theta_i)], \quad |\delta| \le \Delta/S_0\,, \qquad (15)$$

$$Q_{12} = S_0\delta(\theta_i) - Q_2, \quad \langle\delta\rangle = 0\,.$$

Here S_0 is the center of the subsample and $\delta(\theta_i)$ characterizes a (small) random scatter of the pixel amplitudes with respect to the central point. In this case

$$\langle Q_{12}^2\rangle = \langle Q_2^2\rangle - 2S_0\langle\delta S_2\rangle + S_0^2\langle\delta^2\rangle\,,$$

$$\langle Q_2 Q_{12}\rangle = -\langle Q_2^2\rangle + S_0\langle\delta Q_2\rangle, \quad \alpha = \frac{1-o_1(\delta)}{1-o_2(\delta)}$$

$$C(\theta_i) = S_2(\theta_i)(1-\alpha) + \alpha S_0[1+\delta(\theta_i)]\,. \qquad (16)$$

Thus, for $\Delta \to 0$ we get

$$\alpha \to 1 \quad C(\theta_i) \to S_0, \quad \sigma_C^2 \to 0\,. \qquad (17)$$

For such a choice of the function G_i (15), we get an unexpected result - for small $\Delta \to 0$ the signal CMB tends to $\langle S_1\rangle = S_0$. Numerical simulations confirm these tendencies and as is seen from the Table 1 for small Δ the selected signal, C, is close to the input one, S_1, and strongly differs from S_2. For larger Δ this difference disappears.

TABLE I. Examples of the reconstruction of the CMB signal with the model 3 (arbitrary units)

Δ	Npixels	$\langle S_1\rangle$	$\langle S_2\rangle$	$\langle C\rangle$
200μK	256129	8.7 ± 5.40	5.6 ± 5.3	3.3 ± 6.3
2μK	2835	1.0 ± 0.57	-20.0 ± 17.0	0.4 ± 0.8
2μK	2922	3.0 ± 0.60	-18.0 ± 18.0	1.3 ± 1.6

4. Model 4

The most promising results are obtained for the pixel subsample selected with the condition

$$G_i = S_1(\theta_i) - S_2(\theta_i) = F_1(\theta_i) - F_2(\theta_i) = \beta(1+\delta_i) \quad (18)$$

$$Q_{12} = \beta\delta(\theta_i) \quad \langle\delta\rangle = 0, \quad |\delta_i| \le \Delta/\beta\,.$$

Here, β is the center of the subsample and $\delta_i = \delta(\theta_i)$ characterizes a (small) random scatter of the pixel amplitudes with respect to the central point. It is an advantage of this approach that, similarly to the Model 1, the function G_i depends upon the foregrounds only. In this case

$$\langle Q_2 Q_{12}\rangle = \beta\langle S_2\delta\rangle, \quad \langle Q_{12}^2\rangle = \beta^2\langle\delta^2\rangle, \quad \alpha = -\frac{\langle\delta S_2\rangle}{\beta\langle\delta^2\rangle}\,,$$

$$C(\theta_i) = S_2(\theta_i) - [1+\delta(\theta_i)]\langle S_2\delta\rangle/\langle\delta^2\rangle\,, \quad (19)$$

$$\sigma_C^2 = \langle Q_2^2\rangle - \langle S_2\delta\rangle^2/\langle\delta^2\rangle$$

For such a choice of the function G_i, the results depend upon the bin size but even for $\Delta \to 0$ the restored C_i do not tend to the real CMB signal. This means that in this case a very small Δ is not the best choice and the best Δ must be found from simulations.

Examples of such reconstructions of the input CMB signal with $\Delta = 2$, 0.2, & $0.002mK$ are presented in Fig. 2. As is seen from this Figure, the reconstructed signal is weakly sensitive to the small Δ used and oscillates around the level $C_\ell/C_{in} \sim 1. - 1.1$. The scatter of the method depends upon the bin size used, Δ, but does not exceed $\sim 15\%$.

III. POWER SPECTRUM FROM Q AND V BANDS OF THE WMAP MEASUREMENTS

As was found in previous Section, the best reconstruction of the CMB map, $T(\theta_i)$, and the power spectrum, C_ℓ, of the CMB temperature fluctuations is possible with the condition (18). Applying this approach with $\Delta \le 0.2mK$ for the Q and V observed maps, we use from several tens to several thousands of 'homogeneous' regions. To compare properties of our and WMAP CMB maps ($T_4(\theta_i)$ & $T_{WMAP}(\theta_i)$, respectively), we plot in Fig. 3 the PDFs for ratio $x_i = T_4(\theta_i)/T_{WMAP}(\theta_i)$ found for each map pixel. As is seen from this Figure, for $\sim 60\%$ of pixels we have $-0.5 \le x_i \le 2.5$ while for other pixels even larger divergences are seen. For $\Delta = 0.2mK$ & $2\mu K$ these PDFs can be fitted by the Gaussian function

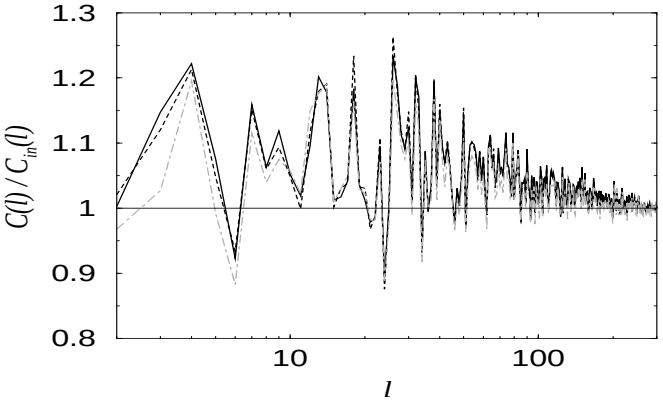

FIG. 2. For the model 4 three reconstructions of modeling CMB signal are plotted for the foregrounds in Q and V bands. Results are normalized on the amplitude of input signal and shown for $\Delta = 2, 0.2mK$ & $2\mu K$ (solid, dashed and dot - dashed lines).

$$P(x) \approx 0.36\exp[-(x-1.16)^2/1.6]\,. \quad (20)$$

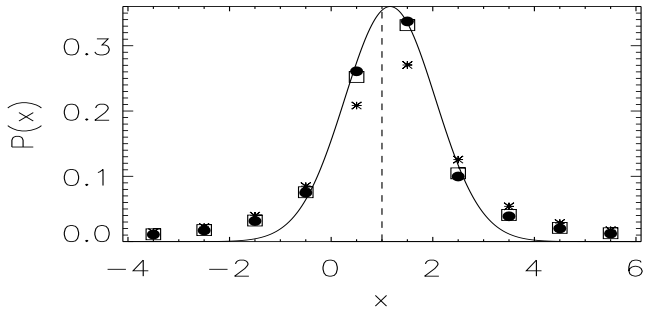

FIG. 3. The PDFs $P(x = T_4/T_{WMAP})$ are plotted for $\Delta = 2mK$, (stars), $\Delta = 0.2mK$, (squares), and $\Delta = 2\mu K$, (points). Fit (20) is plotted by solid line.

The most important physical inferences come from the spectral characteristics of the temperature, a_{lm} & C_ℓ (7). For $\Delta = 2\mu K$ coefficients $a_{\ell m}$ are listed in Table II. For $\Delta = 20\mu K$ our estimates ΔT_ℓ^2 are plotted in Fig. 4.

With these $a_{\ell m}$, we get for the quadrupole and octupole

$$\Delta T_2^2 \approx 1\,077\mu K^2, \quad \Delta T_3^2 \approx 1\,233\,, \quad (21)$$

which are close to theoretical expectations [3] for $\ell = 2$,

$$\Delta T_{th}^2 \approx 1250\mu K^2\,, \quad (22)$$

and exceed estimates obtained by the WMAP team [4],

$$\Delta T_2^2 \approx 240.5\mu K^2, \quad \Delta T_3^2 \approx 1\,049\,. \quad (23)$$

TABLE II. For Q and V bands of the WMAP-7 data, amplitudes of the quadrupole, a_{2m}, and the octupole a_{3m}, are listed in μK. The separation is performed with the condition (18) for $\Delta = 2\mu K$.

	WMAP		Model 4	
m	$\ell = 2$	$\ell = 3$	$\ell = 2$	$\ell = 3$
0	11.77	-6.48	-65.21	1.59
1	-0.77	-12.19	-13.86	-21.50
-1	6.21	2.03	8.97	-0.32
2	-14.12	21.99	-17.34	19.80
-2	-17.94	0.59	-10.98	4.03
3	–	-11.71	–	-7.90
-3	–	33.55	–	36.40

An amplitude of the quadrupole similar to the theoretically expected one (22) was also found in [13].

As is well known, the five quadrupole coefficients are equivalent to the components of a symmetric traceless tensor. For the principle values and orientation of tensor axes for the 3 years WMAP quadrupole we have [21]

$$\lambda_1 = \quad 27.1\mu K, \quad (l,b) = (-0.8^\circ \pm 13^\circ,\ 63.3^\circ \pm 1^\circ)\,,$$

$$\lambda_2 = \quad 12.9\mu K,\ (l,b) = (15.5^\circ \pm 3^\circ,\ \ 25.8^\circ \pm 1.2^\circ), \quad (24)$$

$$\lambda_3 = -40 \ \ \mu K, \quad (l,b) = (-77.6^\circ \pm 5^\circ,\ \ 6.5^\circ \pm 4^\circ)\,,$$

In contrast, for our parameters of the quadrupole we get

$$\lambda_1 = \quad 68.3\mu K, \quad (l,b) = (-75^\circ, \quad 9.1^\circ)\,,$$

$$\lambda_2 = \quad 12.0\mu K, \quad (l,b) = (13.1^\circ, \ -8.7^\circ), \quad (25)$$

$$\lambda_3 = -80.4\mu K, \qquad (l,b) = (60.^\circ, \quad 77.4^\circ)\,,$$

with

$$\Delta T^2 = -\frac{3}{5\pi}(\lambda_1\lambda_2 + \lambda_1\lambda_3 + \lambda_2\lambda_3) = 1077\mu K^2\,.$$

The tensor orientations (25) differ from both the dipole direction

$$(l,b)_D = (-96^\circ, 48^\circ)\,,$$

and from the tensor orientations (24).

As is seen from Fig. 4, the most serious differences are found for $\ell = 2$, 4, and for even $\ell \leq 30$. For these even ℓ our estimates of C_ℓ exceed ones obtained by the WMAP team by a factor of ~ 1.5 what emphasizes the symmetry of the CMB signal in north and south hemispheres. For odd ℓ deviations from the WMAP results do not exceed 10%. For $\ell \geq 30$ all differences become small.

These differences do not distort strongly the main conclusions of the WMAP team which are weakly dependent upon the low ℓ part of the power spectrum. However, they significantly suppress three anomalies presented in the WMAP results. Moreover, the new estimate of C_2 can noticeably change estimates of the quadrupole polarization and, therefore, the redshift of reionization.

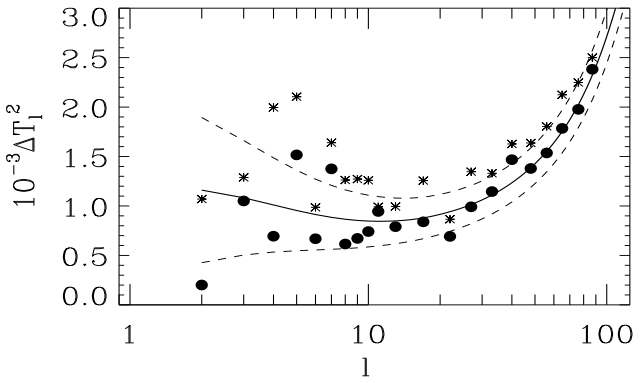

FIG. 4. The $10^{-3}\Delta T_\ell^2$ are plotted for the WMAP data (points) and data obtained under conditions (18) (stars) with $\Delta = 20\mu K$. Solid and dashed lines show the theoretically expected values and their scatter.

IV. SUMMARY AND DISCUSSION

In this paper we considered the application of the ILC approach for analysis of the CMB measurement by the WMAP mission. This approach does not require any additional information on foregrounds which is its great advantage. For the WMAP measurements it can be used for $\ell \leq 100$ where the instrumental noise does not dominate and the amplitudes of measured signals depend upon frequency. However, the ILC method is unstable with respect to the selection of 'homogeneous' subsamples of map pixels and it provides an accurate separation of the CMB signal and foregrounds only for special choices of such 'homogeneous' subsamples.

For measurements of the WMAP mission, the more stable estimates of the CMB fluctuations are obtained for channels Q and V and for the selection criteria (18). Theoretical consideration (19) shows that with these criteria the approximate separation of the CMB signal and foreground can only be obtained. However, the numerical analysis in Fig. 2 demonstrates that for the suitable choice of the bin size, Δ, (6) errors $\delta T/T \leq 10\%$ can be easy achieved.

A. Main results

Main results of our analysis can be summarized as follow:

1. The ILC method is unstable and the resulting CMB characteristics depend strongly upon criteria used for the selection of the 'homogeneous' subsamples of measured signals.

2. Our amplitude of the quarupole exceeds the value given by the WMAP team by a factor of 2.1 which eliminates the disagreement between the theoretically expected and measured values.

3. A comparison of the amplitudes of the quadrupoles, a_{2m}, and the octupoles, a_{3m}, obtained with the WMAP and our approaches (Table II) shows that for our results the effect of the "axes of evil" is substantially reduced.

4. All even C_ℓ with $4 \leq \ell \leq 20$ exceed the values given by the WMAP team by a factor of $\approx 1.5 - 2$ while deviations of odd C_ℓ from the WMAP estimates do not exceed a factor of 1.2 - 1.3. These corrections improve the symmetry of the CMB signal in the north and south hemispheres.

5. For $\ell \leq 20$ an error in the measured $C_\ell \leq 10\%$ is expected. For $\ell \geq 30$ deviations of our estimates from the WMAP results do not exceed $\approx 5\%$.

The best results are obtained for the frequency channels Q & V and are presented in Fig. 4. These results indicate that the main conclusions of the WMAP team remain correct but some of the WMAP anomalies could be caused by admixture of foregrounds to the CMB map. The correction of the large scale characteristics suppresses three anomalies and leads to the moderate correction of the estimates of σ_8. The most important that these corrections change the estimates of the quadrupole polarization and, therefore, the estimates of redshift of reionization of the Universe and formation of earlier galaxies.

It is important that the final estimates of the CMB characteristics depend upon the bin size Δ (6). Thus, for $\Delta \geq 10mK$ our results are quite similar to those obtained by the WMAP team. Correct results are obtained for $\Delta \leq 0.2mK$ only.

The further more detailed analysis of the problem can point to more effective methods of component separation. First of all, this approach can be extended for three and more frequency channels, and the recurrent application of such approach for several pairs of frequency channels can be used. The application of refined technique developed by the WMAP team can also improve results. In particular, the account of correlation of the CMB signal in neighboring pixels can improve the quality of the cleaned CMB map.

With these improvements we can hope to decrease the errors of measured C_ℓ down to the values presented in [4].

B. Methodology

The considered models allow us to obtain some inferences related to the ILC method. Thus, we see that:

1. The best separation is possible by using the foreground measurements (model 1). However, such approach is of no concern for a practice as we do not know *a priori* the foregrounds.

2. Models 2 and 3 demonstrate that with a suitable choice of the selection criteria we can obtain arbitrary estimates for the CMB signal.

3. The best estimates of the CMB signal can be obtained with the selection criteria (18). However, even in this model the CMB signal can be found with errors which depend upon the bin size Δ (6) used for the subsample selection.

4. A comparison of theoretical and numerical estimates of errors for models 3 and 4 shows that sometime the former ones do not characterize adequately the final precision achieved.

Our analysis demonstrates that the final results depend upon the actual foreground. This inference is confirmed by comparison of results obtained for various pairs of frequency channels. A further cleaning of the CMB map can be performed by recurrent application of the proposed method to two or more cleaned maps obtained for different pairs of frequencies. With the WMAP data we can not test this approach as the quality of maps obtained for Q and V channels is much better than the quality of maps found for other frequency channels. However, for many channels of the PLANCK mission [25] such an approach becomes promising.

1. Estimates of the high ℓ power spectrum

As is well known for the real CMB maps with the finite number of pixels, the determination of the power spectrum for larger ℓ is a complex process because the polar regions with relatively small number of pixels along the azimuthal coordinate cannot be used. Hence for high ℓ we would have to analyze regions in the vicinity of the map equator. For a usual map presentations its equator coincides with the most noisy regions of the Galaxy equator what decreases the precision achieved.

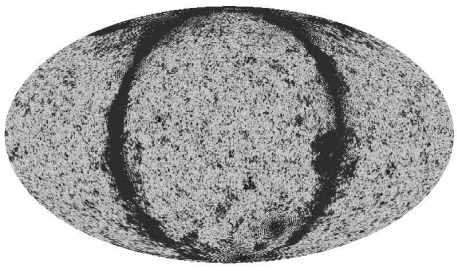

FIG. 5. The CMB map for the Q channel after rotation of the coordinate system.

To decrease the influence of the noisy regions near the galactic equator, we can change the map orientation. Indeed, if we build the map in coordinate system with the galactic equator situated along some map meridian then we have the less noisy area near the map equator while

some of the noisy pixels will be shifted to polar regions. An example of such a map is presented in Fig. 5.

Of course, such approach requires preparation of two different maps one of which have the ordinary orientation and can be used for the analysis of the low ℓ part of power spectrum while the second one with the orthogonal orientation can be used for analysis of high ℓ components of the power spectrum.

This approach seems to be quite effective but it must be tested with real repixelized maps.

V. ACKNOWLEDGMENTS

We thank J.C.B. Papaloizou, P.B. Ivanov, and the anonymous referee for useful comments. We thank NASA for making available the NASA Legacy Archive, where we adopted the WMAP data. We are also grateful to the authors of the HEALPix[1] [22] package, which we has been used to transform the WMAP7 maps into the coefficients $a_{\ell m}$. This work made use of the GLESP [2] [23, 24] package for the further analysis of the CMB data on the sphere. This paper was supported in part by Russian Foundation for Basic research grant Nr. 08-02-00159 and Nr. 09-026-12163, and Federal Program 'Scientific and Pedagogical Personal Innovative of Russia' Nr. 1336. O.V.V. also acknowledges partial support from the "Dynasty" Foundation and the RFBR grant No 09-02-00298.

[1] C. L. Bennett M. Halpern, G. Hinshaw et al., Astrophys. J. Supp. **148**, 1 (2003), astro-ph/0302207.
[2] C. L. Bennett R. S. Hill, G. Hinshaw et al., Astrophys. J. Supp. **148**, 97 (2003), astro-ph/0302208.
[3] D. N. Spergel, L. Verde, H. V. Peiris et al., Astrophys. J. Supp. **148**, 175 (2003), astro-ph/0302209.
[4] G. Hinshaw, M. Nolta, C. Bennet, et al., Astrophys. J. Supp. **170**, 288 (2007), astro-ph/0603451.
[5] D. N. Spergel et al., Astrophys. J. Supp. **170**, 377 (2007), astro-ph/0603449.
[6] G. Hinshaw, J. L. Weiland, R. S. Hill et al., Astrophys. J. Supp. **180**, 225 (2009), arXiv:0803.0732.
[7] E. Komatsu, J. Dunkley, M. R. Nolta et al., Astrophys. J. Supp. **180**, 330 (2009), arXiv:0803.0547.
[8] N. Jarosik, C. L. Bennett, J. Dunkley, et al., Astrophys. J. Supp., submitted (2010), arXiv:1001.4744.
[9] E. Komatsu, K. M. Smith, J. Dunkley, et al., Astrophys. J. Supp., submitted (2010), arXiv:1001.4538
[10] G. Efstathiou, Mon. Not. R. Astron. Soc., **349**, 603, (2004)
[11] M. Tegmark and G. Efstathiou, Mon. Not. R. Astron. Soc., **281**, 1297 (1996)
[12] M. Tegmark M., de Oliveira-Costa and A. Hamilton, Phys. Rev. D, **68**, 123523 (2003)
[13] A. Bonaldi, S. Ricciardi, S. Leach, F. Stivoli, C. Baccigalupi, G. De Zotti, Mon. Not. R. Astron. Soc., 382, 1791, (2008)
[14] J. Kim, P. Naselsky, P. R. Christensen, Phys. Rev. D, **79**, 023003, (2009)
[15] D Maino, S. Donzelli, A. J. Banday, et al. Mon. Not. R. Astron. Soc., **374**, 1207 (2007), astro-ph/0609228.
[16] P. D. Naselsky, O. V. Verkhodanov, and M. T. B. Nielsen. Astrophys. Bull. **63**, 216 (2008), arXiv:0707.1484.
[17] R. Vio & P. Andreani, arXiv:0910.4294
[18] S. M. Leach, J.-F. Cardoso, C. Baccigalupi, et al. Astro. & Astrophys., **491**, 597 (2008), arXiv:0805.0269.
[19] C. Bennet et al. arXiv:1001.4758
[20] B. Gold, N. Odegard, J. L. Weiland, et al. Astrophys. J. Supp., submitted (2010), arXiv:1001.4555.
[21] M.Demiański, A.Doroshkevich, Phys. Rev. D, **75**, 123517, (2007)
[22] K. Górski, E. Hivon, A. J. Banday, B. D. Wandelt, et al., Astrophys. J **622**, 759 (2005).
[23] A. G. Doroshkevich, P. D. Naselsky, O. V. Verkhodanov et al., Int. J. Mod. Phys. D **14**, 275 (2003), astro-ph/0305537.
[24] O. V. Verkhodanov, A. G. Doroshkevich, P. D. Naselsky et al., Bull. SAO **58**, 40 (2005).
[25] Planck early results, arXiv:1101.2038; arXiv:1101.2039

[1] http://healpix.jpl.nasa.gov/

[2] http://www.glesp.nbi.dk